RSC Advances

PAPER

View Article Online
View Journal | View Issue

Cite this: *RSC Adv.*, 2015, **5**, 41941

Soft template mediated synthesis of Bi–In–Zn–S and its efficient visible-light-driven decomposition of methylene blue†

Aniruddha Molla, Meenakshi Sahu, Yogendra Kumar and Sahid Hussain*

Received 21st April 2015
Accepted 23rd April 2015

DOI: 10.1039/c5ra07248d

www.rsc.org/advances

Soft template mediated synthesis of Bi–In–Zn–S (BIZS) nanostructures were successfully achieved in poly(ethylene glycol)-*block*-poly(propylene glycol)-*block*-poly(ethylene glycol) *i.e.* PEG-PPG-PEG at various temperatures with uniform size distributions. The newly synthesized BIZS nanostructures were characterized by powder XRD, IR, UV-vis, SEM, TEM, EDX, BET and TGA. The photocatalytic activities of the BIZS nanostructures were measured by the degradation of methylene blue under visible light (200 W tungsten lamp and sunlight).

1 Introduction

Many interesting physical and chemical properties of nanostructured materials emerge that are significantly different from those of conventional bulk analogs, due to their small size and large surface area.[1] Metal chalcogenides are widely available in nature and among these, Cu-based multinary chalcogenides such as ternary $CuInX_2$ and quaternary Cu_2ZnInX_2 and their alloys, have been subject of immense interest over last five years.[2] These materials have shown promising technological applications in energy conversion, including fuel cells,[3] solar cells,[4] sensors, light-emitting diodes, Li-ion batteries,[5] photoelectrochemical water splitting cells,[6] supercapacitors,[7] thermoelectric devices and memory devices.[8] For example, $CuGaS_2$ and alloyed $(ZnS)_x(CuInS_2)_{1-x}$ has shown a great deal of promise as photocatalysts for the degradation of industrial dye pollutants and excellent water splitting ability.[9] Of late, numerous photocatalysts have been prepared, but only few photocatalyst under visible-light have been reported.[10] Due to these interesting features, researchers have paid attention to synthesize these ternary/quartnary chalcogenides in a facile, convenient, eco-friendly and cost-effective manner. There are several liquid-phase synthetic methods available *e.g.* liquid exfoliation, hot-injection, hydrothermal, solvothermal, microwave, sonochemical, template-directed and colloidal methods for the production of this type of materials. Recently, Xue *et al.* reported a room temperature synthesis of Cu–In–Zn–S (CIZS) using thioacetamide and water.[11] In no denial of fact, some reported methods are creditable but most of suffers from drawbacks like requirement of special set-up for inert condition, use of toxic solvent and foreign substrate as capping agent to control the growth of the nanoparticles. Herein we report a soft template mediated synthesis of Bi–In–Zn–S (BIZS) nanoclusters using different solvent and at different temperatures. The obtained nanoclusters have size ~2–10 nm. The photocatalytic activity of prepared nanoclusters was studied with methylene blue under visible light (200 W tungsten lamp and sunlight).

2 Experimental

2.1 Material

Zinc acetate dihydrate $[Zn(OAc)_2\cdot 2H_2O]$, indium acetate $[In(OAc)_3]$, bismuth nitrate pentahydrate $[Bi(NO_3)_3\cdot 5H_2O]$, poly(ethylene glycol)-400 or PEG-400, glycerol, poly(ethylene glycol)-*block*-poly(propylene glycol)-*block*-poly(ethylene glycol) or PEG-PPG-PEG, thiourea $[CS(NH_2)_2]$, ethanol (EtOH) and methylene blue were all analytical grade and used without further purifications. Double distilled water was employed throughout the experiments.

2.2 Preparation of BIZS nanoclusters

In a typical experiment, $Zn(OAc)_2\cdot 2H_2O$ (2.5 mmol, 549 mg), $In(OAc)_3$ (1.0 mmol, 292 mg), and $Bi(NO_3)_3\cdot 5H_2O$ (0.3 mmol, 146 mg) were taken in 100 ml round bottom flask with 10 ml of solvent [PEG-PPG-PEG (sample B, C and D), PEG-400 (sample E) or glycerol (sample F)]. The reaction mixture was stirred at different temperatures [150 °C for all the solvents, 100 °C (sample B) and 200 °C (sample D) for PEG-PPG-PEG only] for 1 h. The solution become white and excess thiourea (400 mg) was added in it. The solution turned to light yellow and finally black after 3 hours of stirring. It was kept at room temperature to cool down and sample was collected by centrifugation, washed several times with ethanol and water. Finally the dark mass was collected and dried under vacuum. Details flow chart for the

Department of Chemistry, Indian Institute of Technology Patna, Patna 800 013, India. E-mail: sahid@iitp.ac.in; Fax: +91-612-227-7383; Tel: +91-612-255-2022

† Electronic supplementary information (ESI) available: Spectral data of all compounds are available. See DOI: 10.1039/c5ra07248d

synthesis of BIZS at various temperatures can be seen in Fig. S1 (ESI†).

2.3 Characterizations methods of catalyst

IR spectra were recorded in KBr on a Shimadzu IR Afinity I. SEM images were obtained from a Hitachi S-4800 microscope at an operating voltage of 15 kV. The sample was coated with platinum for effectual imaging before being charged. TEM images were obtained from JEOL instrument using Cu grid. UV-vis and fluorescence data was recorded in UV-vis spectrophotometers of Shimadzo UV-2550 using standard 1 cm quartz cuvette and Fluoromax-4 spectrofluorometer of Horiba Jobin YVON respectively. X-ray powder diffraction study was carried out on a Rigaku X-ray diffractometer at a voltage of 35 kV using Cu Kα radiations ($\lambda = 0.15418$ nm) at scanning rate of 0.20° per minute in the 2θ range 10–80°. BET measurement was performed using Smart Instruments; Smart Sorb 92/93 and finally TGA experiment was carried out in SDT Q600.

2.4 Photocatalytic experiments

In order to evaluate the photocatalytic activities of the prepared BIZS nanoclusters, the photocatalytic decomposition of methylene blue (MB) under visible light (200 W tungsten lamp and sunlight) irradiation was investigated. 5 mg of prepared BIZS was dispersed in 14 ml aqueous solution of 5×10^{-5} (M) MB. Before irradiations, the suspensions were magnetically stirred for 20 min in the dark in order to reach the adsorption–desorption equilibrium between the catalyst and dye molecule. Then the mixture was exposed to visible-light irradiations from a 200 W tungsten lamp or sunlight (for the sample prepared at 200 °C *i.e.* sample D) with continuous stirring. At given time interval, 2 ml aliquots were taken and were centrifuged to remove the catalyst. UV-vis spectra were recorded with 1 : 1 dilution of experimental solution taken at certain interval. Blank experiments were also performed under identical conditions. The effective solar global energy was measured using pyranometer for comparative study with sunlight and 200 W lamp.

2.5 X-ray diffraction (XRD)

Powder XRD patterns of the BIZS nanoclusters prepared at different temperature and in different solvents are shown in Fig. 1. The diffraction peaks (2θ) of BIZS nanoclusters at 28.62° (111), 47.56° (220) and 55.20° (311) are reliable with the reported chalcopyrite structure of Cu–In–Zn–S (JCPDS no. 65-0309).

When BIZS are synthesised at 100 °C and 150 °C, additional diffraction peaks are obtained at near 28.62° which is due to the formation of individual metal sulphide. We further compared our results with the corresponding individual metal sulphide. It is clear from the XRD data that in case of sample prepared at 100 °C using PEG-PPG-PEG as solvent (Fig. 1B), the nanoclusters are In_2S_3 rich (ESI, Fig. S2H†) whereas for the sample prepared at 150 °C (Fig. 1C) it is Bi_2S_3 (ESI, Fig. S2G†). Impurities of individual metal sulphides were also observed when the synthesis is carried out in polyethylene glycol-400 (PEG-400) (Fig. 1E) and glycerol (Fig. 1F) at 150 °C. The individual metal

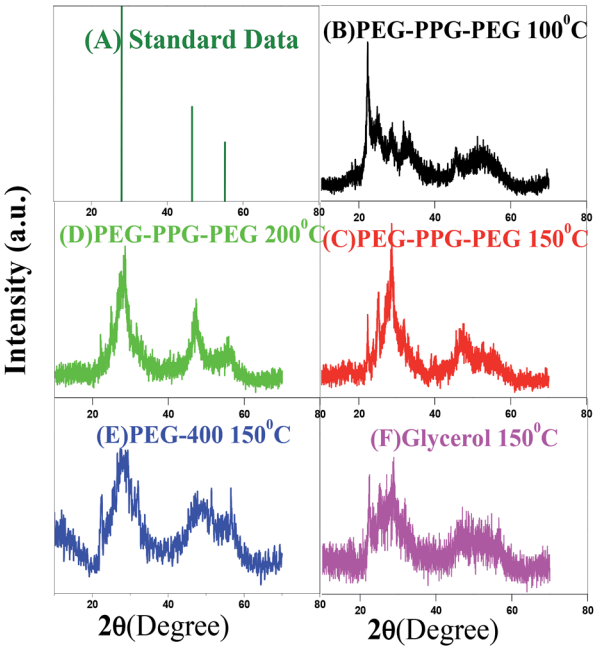

Fig. 1 P-XRD of BIZS prepared at various temperature and solvent.

sulphide formation is more favourable at relatively low temperature,[12] than ternary and quaternary chalcogenides.

2.6 Infrared spectroscopy (FT-IR)

FT-IR of the all BIZS sample is revealed in Fig. 2. All the samples show peaks at ~3313, 1557, 1426 and 1014 cm^{-1}. These peaks are nearly in the same region and are due to similar nature of the solvent which was used for the synthesis of BIZS at various temperatures. A very weak metal-sulfur bands can be seen in the spectrum over 550–400 cm^{-1} together with the surface bonded solvents' characteristic peak in the region of 1500–1000 and at 3200–3400 cm^{-1}. The solvents used for the synthesis are PEG-PPG-PEG, PEG-400 and glycerol, which has very similar types of functional groups and bonds (–OH, $–CH_2$, and C–O) and as a results IR-spectra shows similar bands.

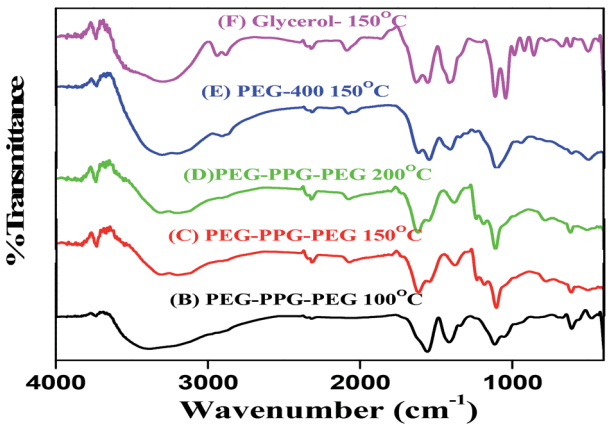

Fig. 2 IR spectra of BIZS prepared at various temperature and solvent.

2.7 The morphologies of the synthesized BIZS using FESEM

The morphologies of the synthesized BIZS were then characterized using FESEM. Thus, the composition one of the BIZS (sample D) was preferred as the example to present the morphology. It shows uniform distributions of nanoclusters (Fig. 3a). More detailed structural information about the clusters (Fig. 3b) was observed in higher magnifications where a large number of nearly identical nanoclusters of size 30–50 nm are observed. All BIZS shows similar morphology although it was synthesised at different temperatures and solvents. SEM study of the sample B showed the presence of nano-rod along with the nanoclusters. It is assumed that there are Bi_2S_3 which forms nano-rod (ESI, Fig. S3B†).[13] Sample E and F also show uniform particle distribution (ESI, Fig. S5 and S6†). The particles are agglomerated in all cases because this is a soft template mediated synthesis using a viscous solvent *i.e.* PEG-PPG-PEG, glycerol and PEG-400. In addition, the morphology of the as-synthesized BIZS was further studied by TEM. Fig. 4 show the TEM images of the nanocluster (sample D). The distributions of particle in nanoclusters with 1–2 nm in size was observed and this was further supported by calculated crystallite size using Scherrer equation. Fig. S7 (ESI†) was the EDX result which confirmed that the compositions of the nanoclusters were Bi, In, Zn and S. To further study the spatial homogeny of the elemental distribution of the obtained nanoclusters, the line profile of the BIZS was measured and composition was found to be $Bi_{0.13}InZn_{1.06}S_{2.59}$ (ESI, Table S1†). The EDX elemental mapping and line mapping further indicated the homogeneous distribution of Bi, In, Zn and S elements throughout the whole sample Fig. 3c.

2.8 Spectral study of BIZS

For UV study, 1 mg of prepared BIZS was dispersed in 10 ml water under sonication. All five samples give similar type of spectra in UV-visible regions with shoulder at ~312 nm (Fig. 5F) for sample F and at ~275 nm (Fig. 5C and E) for sample C and E.

Direct band gap was measured, taking 1 mg of dispersed sample D in 10 ml water with the help of this power equation[14] verses photon energy ($h\nu$).

$$(\varepsilon h\nu)^n = k_d(h\nu - E_g)$$

where k_d is the absorption constant for an direct transition, n is 2 for an direct transition $h\nu$ is the absorption energy, and E_g is the band-gap energy.

Fig. 6 represents the UV-vis absorbance spectrum of sample D, and inset represent $(\varepsilon h\nu)^2$ *versus* $h\nu$ curve of the same sample, where ε is the absorbance coefficient, h the Planck constant and ν the frequency. The direct band gap (E_g) of the BIZS nanoparticle was determined to be at 2.27 eV.

To measure the fluorescence spectra, sample was excited at 350, and emission peak was observed at 421 nm (Fig. 7). For the sample B and F, very low intense fluorescence emission peak at 395 nm was observed but rest of the sample shows intense emission peak at 421 nm along with shoulder at 395 nm.

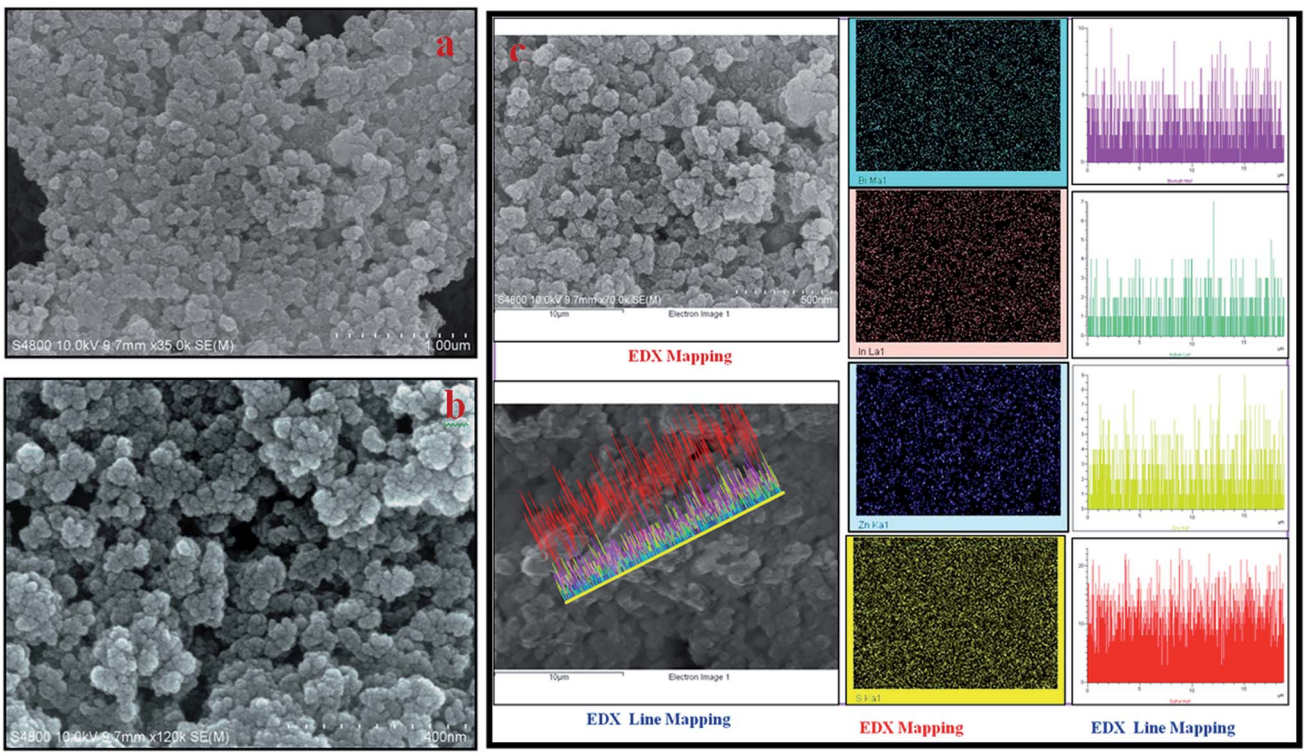

Fig. 3 Morphological study of BIZS prepared at 200 °C (sample D). (a). Low magnification FE-SEM image of BIZS, (b) FE-SEM image of BIZS at 400 nm, (c) EDX spectra of BIZS with elemental and line mapping.

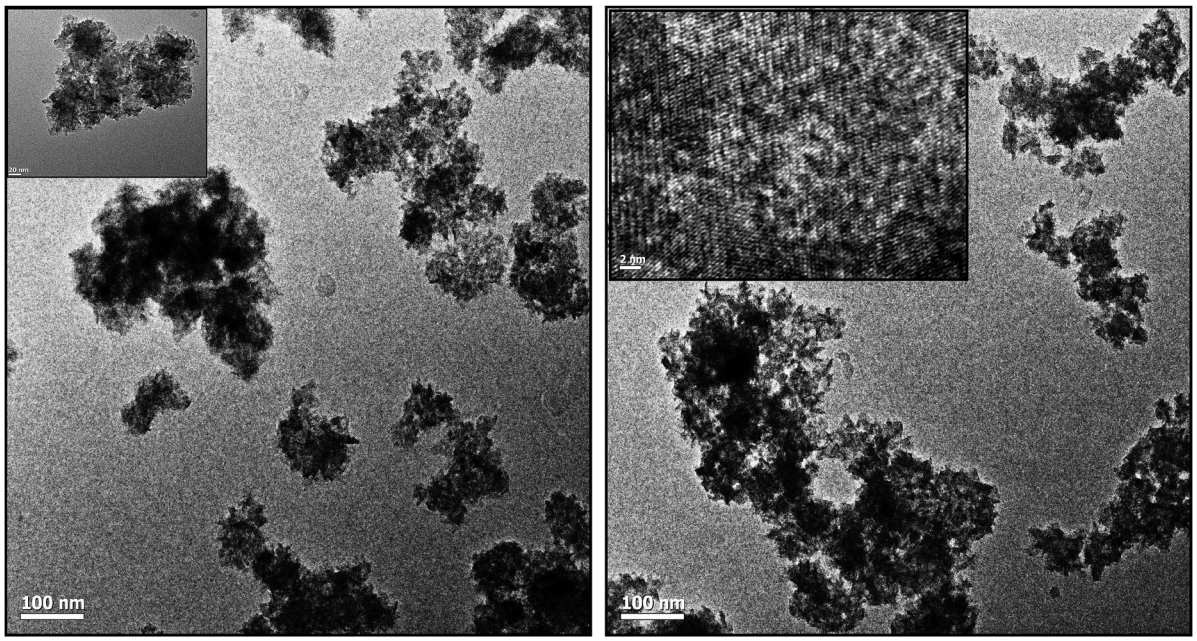

Fig. 4 TEM image of BIZS (sample D) at different magnification.

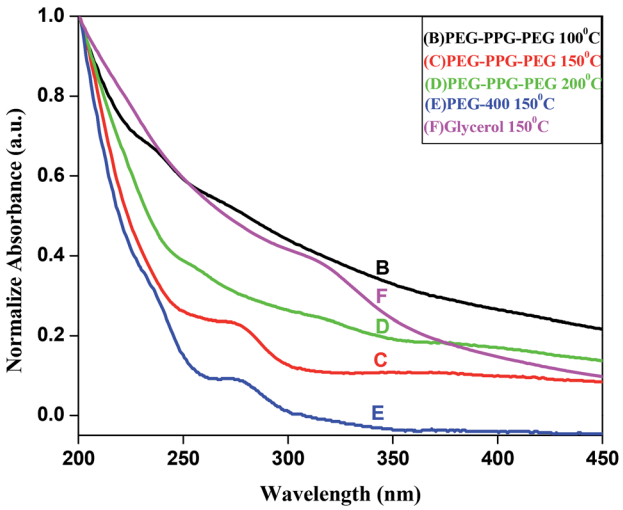

Fig. 5 UV-vis spectra of BIZS prepared at various temperature.

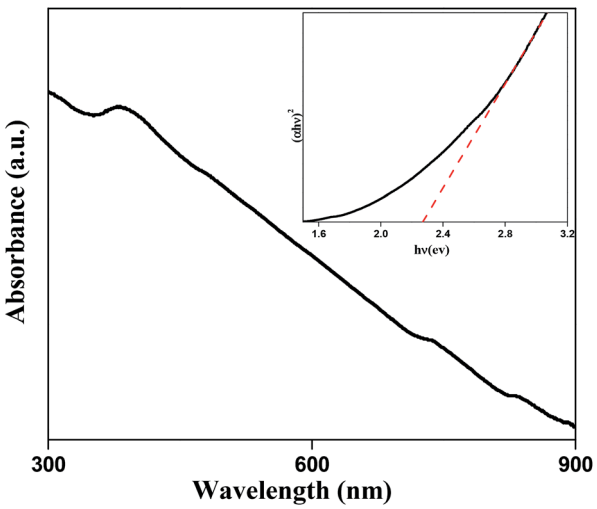

Fig. 6 $(\varepsilon h\nu)^2$ *versus* $h\nu$ curve of BIZS was prepared at 200 °C using PEG-PPG-PEG as solvent.

2.9 BET measurement: surface area analysis

The nitrogen adsorption–desorption was measured using Smart Instrument, Model No-Smart Prob 92/93 to determine the surface area of the obtained BIZS nanoclusters. For this measurement sample was regenerated at 250 °C for two hours. Experiment was performed using N_2 (30%) and He (70%) mixture. The obtained result are summarised in Table 1. It is clear that, the sample B have maximum surface area 99.86 Sq. m g^{-1} whereas sample E shows minimum surface area 20.03 Sq. m g^{-1}. Moderate surface areas were observed for the sample C, D and F. The obtained graph for the analysis is in Fig. S8 (ESI†).

2.10 Thermogravimetric analysis (TGA)

The thermal stability of the BIZS nanoclusters was measured using TGA. All samples were heated up to 750 °C with heating rate 10 °C min^{-1}. The initial weight loss below 200 °C is due to evaporation of physisorbed moisture. A sharp decrease in mass of the samples between 350–415 °C indicates the weight loss due to organics (surface bonded solvents) and sublimation of metal sufides (Fig. 8a). From the derivative plot of TGA graph (Fig. 8b), it is clear that the maximum decay occurs at 370–420 °C. The degradation temperature and weight loss are calculated and is depicted in Table S2 (ESI†). It is clear from the graph and table that sample B, C and F follow a decay pattern that has mass loss

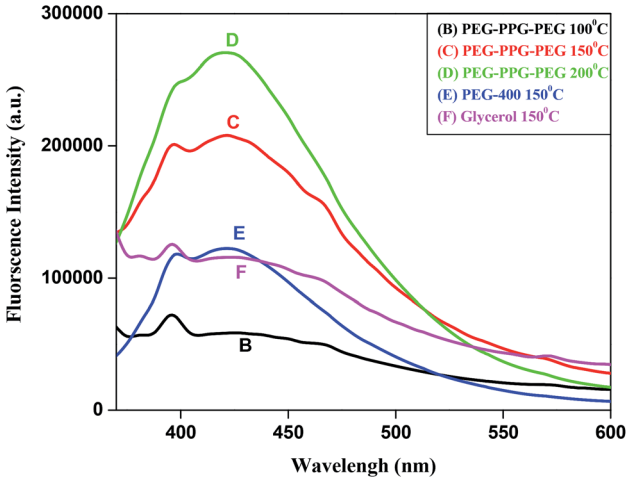

Fig. 7 Fluorescence spectra of BIZS prepared at various temperature and solvent.

at two different temperatures while sample D and E has one decay pattern. This two step decay pattern of sample B, C and F may be due to the impurities (individual metal sulphides) which were also supported by powder XRD data.

2.11 Photocatalytic activities

MB, a stable dye has a characteristic absorption band at 663 nm, which is employed to assess the photocatalytic reactivity of these prepared BIZS nanoclusters. As shown in Fig. S9 (ESI†), the concentrations of MB under 200 W lamp remain almost constant (97%) throughout the experimental time in absence of catalyst whereas under sunlight 15% MB degradation occurs (ESI, Fig. S10†). Initially we started photocatalytic study under 200 W lamp in presence of sample B and F, it shows very weak photocatalytic activities under 200 W lamp (ESI, Fig. S11 and S12†). When the same reaction was performed with sample C and E, moderate photocatalytic activities were observed (ESI, Fig. S13 and S14†). While studying the same reaction with sample D under 200 W lamp and sunlight, the reactions were faster. Nearly 94% (under sunlight) and 92% (200 W lamp) of MB was degraded within 95 min (Fig. 9). In both the cases we observed parallel photodegradation of MB dye and the inset show the visible change in colour of MB from blue to colourless under 200 W lamp.

Various control experiments were performed to check the role of Bi. Pure Bi_2S_3 and Zn–In–S semiconductor were prepared under same reaction conditions. The photocatalytic activity of pure Bi_2S_3 and Zn–In–S were performed with same concentration of MB in presence of 200 W lamp. There was no significant decrease in MB intensity for Bi_2S_3 (Fig. S15, ESI†) whereas with

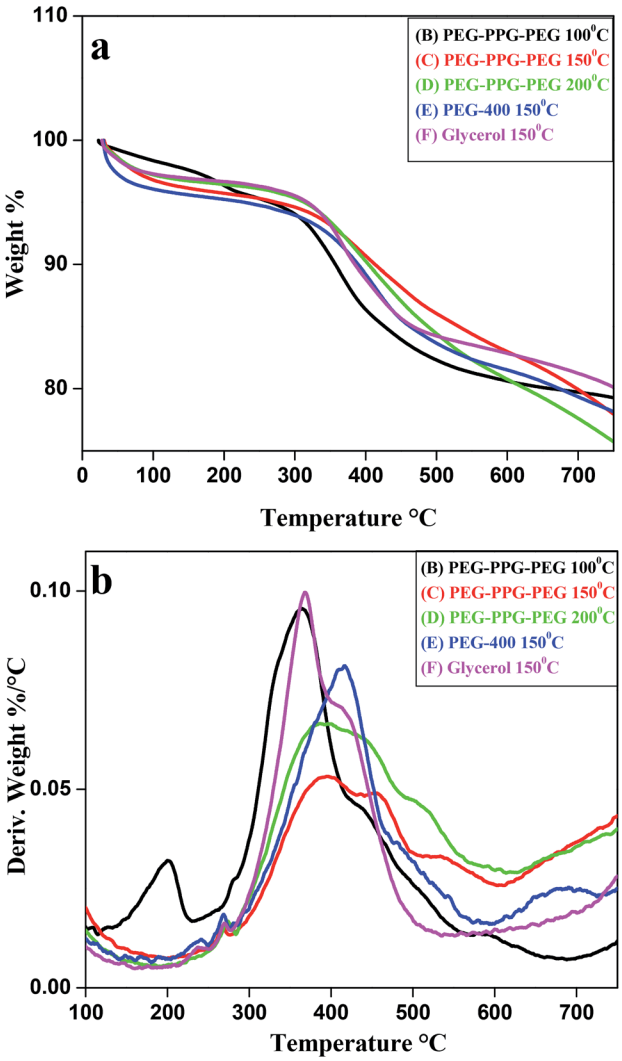

Fig. 8 Thermogravimetric analysis of prepared BIZS, (a) normal plot, (b) derivative plot.

Table 1 Degradation of methylene blue in presence of prepared BIZS and there surface area

Sl. no.	Catalyst	$C_{t=50\ min}$	$C_{t=80\ min}$	C_0	Rate constant (s^{-1}) $\sim 10^{-4}$		Surface area (Sq. m g^{-1})
					$t = 50$ min	$t = 80$ min	
1	(B) PEG-PPG-PEG 100 °C	1.438	1.395	1.617	0.391	0.307	99.86
2	(C) PEG-PPG-PEG 150 °C	0.654	0.385		3.017	2.989	24.18
3	(E) PEG-400 150 °C	0.619	0.373		3.195	3.051	57.13
4	(F) Glycerol 150 °C	1.360	1.318		0.576	0.425	20.03
5	(D) PEG-PPG-PEG 200 °C (sunlight)	0.641	0.165		3.084	4.754	50.32
6	(D) PEG-PPG-PEG 200 °C (200 W tungsten lamp)	0.706	0.146		2.762	5.009	

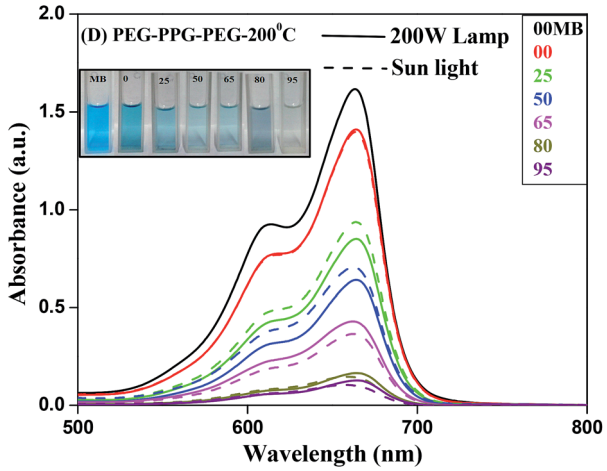

Fig. 9 Time dependent UV-vis spectra of MB in presence of BIZS prepared at 200 °C using PEG-PPG-PEG as solvent under sunlight and 200 W lamp.

freshly prepared Zn–In–S under the similar reaction condition; it did not show any photocatalytic activity. This concludes that Bi_2S_3 and Zn–In–S are not the active component for the decomposition of MB in the present case. This degradation was observed only for BIZS. Comparative studies with different bismuth content are carried out (Fig. S16–S19, ESI†) and it is found to be more effective when it is less than 10%.

The variation of MB concentrations (C/C_0) with irradiation time over different BIZS is shown in Fig. 10, where C_0 is the initial MB concentration before irradiation and C is the MB concentration at time t. In absence of light the decrease in concentration is due to adsorption and desorption process between catalysts and dye. It is evident from Table 1 and the Fig. S20 (ESI†) that degradation of MB in presence of catalysts is a pseudo first order reaction and it follows the activity sequence as D(sun) ~ D(lamp) > E(lamp) > C(lamp) > F (lamp) > B(lamp).

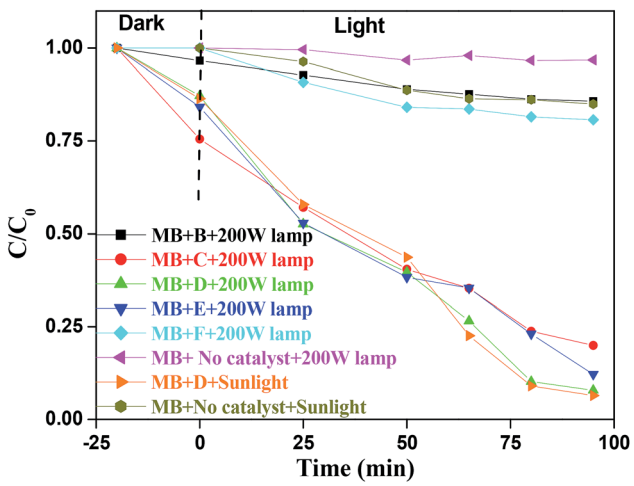

Fig. 10 Photodegradations of MB, (C/C_0) *versus* irradiation time under visible light.

Finally, reusability of catalyst was performed under sunlight and 200 W lamp for the sample D. After complete of one cycle, catalyst was collected by centrifugation, washed several times with ethanol and water and finally dried under vacuum and was in reused for next run. There is no noteworthy decrease in photocatalytic activity after successfully five run in same reactions conditions (Fig. 11).

The possible photocatalytic mechanism is shown in Fig. 12. On radiation of light to the sample, it absorbs light and electrons of valence band are excited to conduction band and generate pairs of electrons and holes on the surface of the catalyst. The positive-hole splits the water molecule into hydroxyl radical. The negative-electron reacts with oxygen molecule to form super oxide anion. The super oxide formation was also confirmed using a non-fluorescent dihydrorhodamine 123 (DHR123) as a Reactive Oxygen Species (ROS) tracking agent.[15] BIZS is non-fluorescent at the wavelength 521 nm. DHR 123 with sample D shows fluorescence intensity after irradiation of light while no change in the fluorescence intensity of DHR 123 without catalyst was observed on irradiation. It is

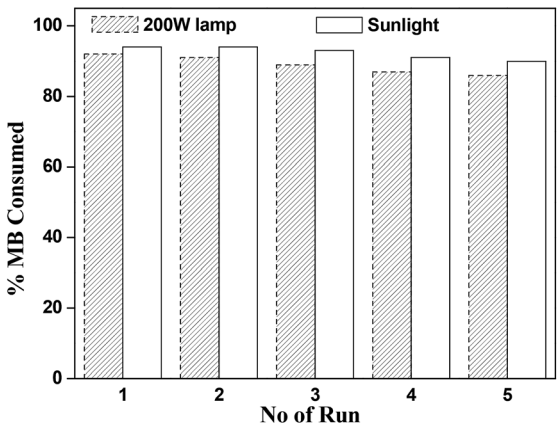

Fig. 11 Photodegradation cycle of BIZS (D) in presence of visible light.

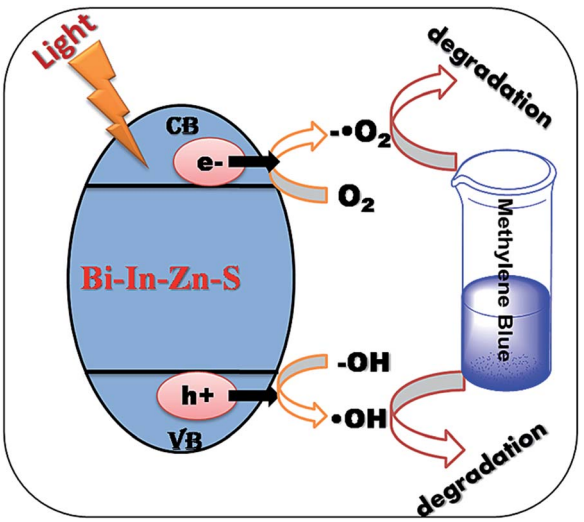

Fig. 12 Photodegradation mechanism of BIZS in presence of light.

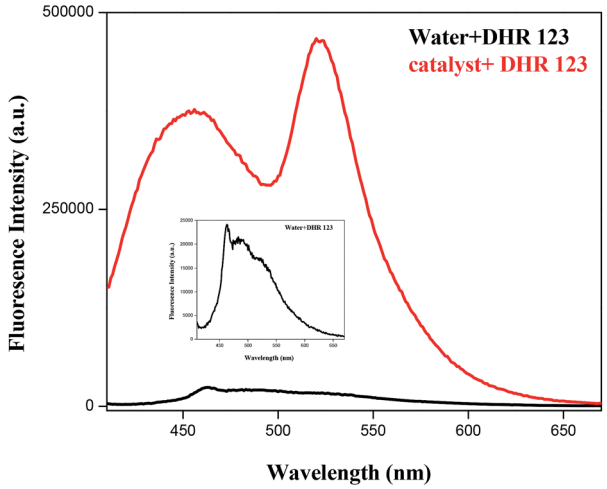

Fig. 13 ROS formation in presence of sample D under light (200 W).

assumed that after irradiation with light, upon reaction with ROS, DHR 123 converted to fluorescent Rhodamine 123. Increase in the intensity of irradiation induced fluorescence due to slow oxidation of DHR 123 in presence of ROS (Fig. 13). It is now clear that the ROS (hydroxyl anion and super oxide anion) forms in presence of catalyst which is responsible for the degradation the methylene blue.

4 Conclusions

In conclusion, we develop a simple and reproducible one-pot soft template medicated protocol for the synthesis of Bi–In–Zn–S nanoclusters using PEG-PPG-PEG as solvent at 200 °C. The obtained nanoclusters of BIZS are characterized by powder XRD, IR, UV-vis, SEM, TEM, EDX, BET and TGA. We explore the photocatalytic activities of BIZS by the degradation of methylene blue under visible light (200 W tungsten lamp and sunlight). The photodegradations are repetitive and effective up to five cycles.

Acknowledgements

A.M and M.S. are thankful to IIT Patna for their research fellowship. Authors are thankful to Department of Science and Technology India for research grant no. SR/FT/CS-093/2009.

Notes and references

1 (*a*) M.-Q. Yang, B. Weng and Y.-J. Xu, *J. Mater. Chem. A*, 2014, **2**, 1710–1720; (*b*) A. Singhal, M. R. Pai, R. Rao, K. T. Pillai, I. Lieberwirth and A. K. Tyagi, *Eur. J. Inorg. Chem.*, 2013, 2640–2651; (*c*) C. Hayashi, *Phys. Today*, 1987, **40**, 44–51; (*d*) H. Gleiter, *Prog. Mater. Sci.*, 1989, **33**, 223–315; (*e*) R. Uyeda, *Prog. Mater. Sci.*, 1991, **35**, 1–18.

2 (*a*) L. A. Koscielski and J. A. Ibers, *Z. Anorg. Allg. Chem.*, 2012, **638**, 2585–2593; (*b*) M. Afzaal, M. A. Malik and P. O'Brien, *J. Mater. Chem.*, 2010, **20**, 4031–4040; (*c*) M.-R. Gao, Y.-F. Xu, J. Jiang and S.-H. Yu, *Chem. Soc. Rev.*, 2013, **42**, 2986–3017; (*d*) J. Kolny-Olesiak and H. Weller, *ACS Appl. Mater. Interfaces*, 2013, **5**, 12221–12237 and references cited therin.

3 (*a*) Z. Chen, D. Higgins, A. Yu, L. Zhang and J. Zhang, *Energy Environ. Sci.*, 2011, **4**, 3167–3192; (*b*) F. J. Rodriguez, P. J. Sebastian, O. Solorza and R. Perez, *Int. J. Hydrogen Energy*, 1998, **12**, 1031–1035; (*c*) L. Zhang, J. Zhang, D. P. Wilkinson and H. Wang, *J. Power Sources*, 2006, **156**, 171–182; (*d*) Y. J. Wang, D. P. Wilkinson and J. J. Zhang, *Chem. Rev.*, 2011, **111**, 7625–7651; (*e*) N. G. Sahoo, Y. Z. Pan, L. Li and S. H. Chan, *Adv. Mater.*, 2012, **24**, 4203–4210; (*f*) F. Y. Cheng and J. Chen, *Chem. Soc. Rev.*, 2012, **41**, 2172–2192.

4 (*a*) Q. Guo, G. M. Ford, W.-C. Yang, B. C. Walker, E. A. Stach, H. W. Hillhouse and R. Agrawal, *J. Am. Chem. Soc.*, 2010, **132**, 17384–17386; (*b*) K. Jimbo, R. Kimura, T. Kamimura, S. Yamada, W. S. Maw, H. Araki, K. Oishi and H. Katagiri, *Thin Solid Films*, 2007, **515**, 5997–5999; (*c*) Q. Guo, H. W. Hillhouse and R. Agrawal, *J. Am. Chem. Soc.*, 2009, **131**, 11672–11673; (*d*) V. K. Kapur, B. M. Basol and E. S. Tseng, *Sol. Cells*, 1987, **21**, 65–72; (*e*) K. Orgassa, H. W. Schock and J. H. Werner, *Thin Solid Films*, 2003, **431–432**, 387–391; (*f*) S. E. Habas, H. A. S. Platt, F. A. M. van Hest and D. S. Ginley, *Chem. Rev.*, 2010, **110**, 6571–6594; (*g*) P. V. Kamat, K. Tvrdy, D. R. Baker and J. G. Radich, *Chem. Soc. Rev.*, 2010, **110**, 6664–6688; (*h*) G. Q. Zhang, S. Finefrock, D. X. Liang, G. G. Yadav, H. R. Yang, H. Y. Fang and Y. Wu, *Nanoscale*, 2011, **3**, 2430–2443.

5 (*a*) J.-Z. Wang, L. Lu, M. Lotya, J. N. Coleman, S.-L. Chou, H.-K. Liu, A. I. Minett and J. Chen, *Adv. Energy Mater.*, 2013, **3**, 798–805; (*b*) Z. Su, K. Sun, Z. Han, F. Liu, Y. Lai, J. Li and Y. Liu, *J. Mater. Chem.*, 2012, **22**, 16346–16352; (*c*) L. W. Ji, Z. Lin, M. Alcoutlabi and X. W. Zhang, *Energy Environ. Sci.*, 2011, **4**, 2682–2699; (*d*) Z. G. Yang, J. L. Zhang, M. C. W. Kintner-Meyer, X. C. Lu, D. W. Choi and J. P. Lemmon, *Chem. Rev.*, 2011, **111**, 3577–3613.

6 (*a*) M. G. Walter, E. L. Warren, J. R. Mckone, S. W. Boettcher, Q. X. Mi, E. A. Santori and N. S. Lewis, *Chem. Rev.*, 2010, **110**, 6446–6473; (*b*) A. Kudo and Y. Miseki, *Chem. Soc. Rev.*, 2009, **38**, 253–278; (*c*) M. Gratzel, *Nature*, 2001, **414**, 338–344; (*d*) W. J. Youngblood, S.-H. A. Lee, Y. Kobayashi, E. A. Hernandez-Pagan, P. G. Hoertz, T. A. Moore, A. L. Moore, D. Gust and T. E. Mallouk, *J. Am. Chem. Soc.*, 2009, **131**, 926–927; (*e*) G. Wang, H. Wang, Y. Ling, Y. Tang, X. Yang, R. C. Fitzmorris, C. Wang, J. Z. Zhang and Y. Li, *Nano Lett.*, 2011, **11**, 3026–3033; (*f*) O. Khaselev and J. A. Turner, *Science*, 1998, **280**, 425–427; (*g*) M. G. Walter, E. L. Warren, J. R. McKone, S. W. Boettcher, Q. Mi, E. A. Santori and N. S. Lewis, *Chem. Rev.*, 2010, **110**, 6446–6473.

7 (*a*) P. Simon and Y. Gogotsi, *Nat. Mater.*, 2008, **7**, 845–854; (*b*) K. Naoi, W. Naoi, S. Aoyagi, J. I. Miyamoto and T. Kamino, *Acc. Chem. Res.*, 2013, **46**, 1075–1083; (*c*) M. D. Stoller and R. S. Ruoff, *Energy Environ. Sci.*, 2010, **3**, 1294–1301; (*d*) L. L. Zhang and X. S. Zhao, *Chem. Soc. Rev.*, 2009, **38**, 2520–2531; (*e*) G. P. Wang, L. Zhang and J. J. Zhang, *Chem. Soc. Rev.*, 2012, **41**, 797–828; (*f*) A. Ghosh and Y. H. Lee,

ChemSusChem, 2012, **5**, 480–499; (*g*) Y. Huang, J. J. Liang and Y. S. Chen, *Small*, 2012, **8**, 1805–1834; (*h*) Q. Wang, L. Jiao, H. Du, J. Yang, Q. Huan, W. Peng, Y. Si, Y. Wang and H. Yuan, *CrystEngComm*, 2011, **13**, 6960–6963; (*i*) M.-R. Gao, Y.-F. Xu, J. Jiang and S.-H. Yu, *Chem. Soc. Rev.*, 2013, **42**, 2986–3017; (*j*) T. Zhu, B. Xia, L. Zhou and X. W. (David) Lou, *J. Mater. Chem.*, 2012, **22**, 7851–7855; (*k*) H. Wang and H. Dai, *Chem. Soc. Rev.*, 2013, **42**, 3088–3113.

8 (*a*) M. R. Gao, J. Jiang and S. H. Yu, *Small*, 2012, **8**, 13–27; (*b*) C. H. Lai, M. Y. Lu and L. J. Chen, *J. Mater. Chem.*, 2012, **22**, 19–30; (*c*) P. D. Antunez, J. J. Buckley and R. L. Brutchey, *Nanoscale*, 2011, **3**, 2399–2411; (*d*) R. Y. Wang, J. P. Feser, X. Gu, K. M. Yu, R. A. Segalman, A. Majumdar, D. J. Milliron and J. J. Urban, *Chem. Mater.*, 2010, **22**, 1943–1945; (*e*) H. Dittrich, A. Bieniok, U. Brendel, M. Grodzicki and D. Topa, *Thin Solid Films*, 2007, **515**, 5745–5750; (*f*) T. Siegrist, P. Merkelbach and M. Wuttig, *Annu. Rev. Condens. Matter Phys.*, 2012, **3**, 215–237; (*g*) Y. Zhang, M. L. Snedaker, C. S. Birkel, S. Mubeen, X. Ji, Y. Shi, D. Liu, X. Liu, M. Moskovits and G. D. Stucky, *Nano Lett.*, 2012, **12**, 1075–1080; (*h*) M. J. Manos and M. G. Kanatzidis, *Inorg. Chem.*, 2009, **48**(11), 4658–4660; (*i*) A. Sahu, L. Qi, M. S. Kang, D. Deng and D. J. Norris, *J. Am. Chem. Soc.*, 2011, **133**, 6509–6512.

9 (*a*) G. Ma, Z. Lei, H. Yan, X. Zong and C. Li, *Chin. J. Catal.*, 2009, **30**, 73; (*b*) W. Zhang and X. Zhong, *Inorg. Chem.*, 2011, **50**, 4065–4072; (*c*) C. Ye, M. D. Regulacio, S. H. Lim, Q. H. Xu and M. Y. Han, *Chem.–Eur. J.*, 2012, **18**, 11258–11263; (*d*) M. D. Regulacio, C. Ye, S. H. Lim, Y. Zheng, Q.-H. Xu and M.-Y. Han, *CrystEngComm*, 2013, **15**, 5214–5217; (*e*) J. Tian, Z. Zhao, A. Kumar, R. I. Boughton and H. Liu, *Chem. Soc. Rev.*, 2014, **43**, 6920–6937; (*f*) S. Shen and Q. Wang, *Chem. Mater.*, 2013, **25**, 1166–1178; (*g*) Z. Zhao, J. Tian, D. Wang, X. Kang, Y. Sang, H. Liu, J. Wang, S. Chen, R. I. Boughton and H. Jiang, *J. Mater. Chem.*, 2012, **22**, 23395–23403; (*h*) Z. Ma, Z. Yi, J. Sun and K. Wu, *J. Phys. Chem. C*, 2012, **116**, 25074–25080; (*i*) S. Chen and L.-W. Wang, *Chem. Mater.*, 2012, **24**, 3659–3666.

10 (*a*) P.-Y. Lee, H.-S. Tengb and C.-S. Yeh, *Nanoscale*, 2013, **5**, 7558–7563; (*b*) Y. Dong, C. Feng, P. Jiang, G. Wang, K. Li and H. Miao, *RSC Adv.*, 2014, **4**, 7340–7346; (*c*) M. Zhu and G. Diao, *J. Phys. Chem. C*, 2011, **115**, 18923–18934; (*d*) Y. Gao, Z. Zheng, F. Yang, F. Zhang, P. Li, W. Fa, H. Jia and H. Zhao, *CrystEngComm*, 2011, **13**, 1441–1445; (*e*) B. Hu, F. Cai, H. Shen, M. Fan, X. Yan, W. Fan, L. Xiao and W. Shi, *CrystEngComm*, 2014, **16**, 9255–9265; (*f*) X. Zhang, G. Lian, S. Zhang, D. Cui and Q. Wang, *CrystEngComm*, 2012, **14**, 4670–4676; (*g*) M. Wang, Y. Zhang, Y. Zhou, F. Yang, E. J. Kim, S. H. Hahn and S. G. Seong, *CrystEngComm*, 2013, **15**, 754–763; (*h*) W. Li, M. Li, S. Xie, T. Zhai, M. Yu, C. Liang, X. Ouyang, X. Lu, H. Li and Y. Tong, *CrystEngComm*, 2013, **15**, 4212–4216.

11 X. Tang, Q. Tay, Z. Chen, Y. Chen, G. K. L. Goh and J. Xue, *New J. Chem.*, 2013, **37**, 1878–1882.

12 J. K. Olesiak and H. Weller, *ACS Appl. Mater. Interfaces*, 2013, **5**, 12221–12237.

13 (*a*) V. Kaltenhauser, T. Rath, W. Haas, A. Torvisco, S. K. Müller, B. Friedel, B. Kunert, R. Saf, F. Hofer and G. Trimmel, *J. Mater. Chem. C*, 2013, **1**, 7825–7832; (*b*) J. L. T. Chen, V. Nalla, G. Kannaiyan, V. Mamidala, W. Ji and J. J. Vittal, *New J. Chem.*, 2014, **38**, 985–992; (*c*) R. Chen, M. H. So, C.-M. Che and H. Sun, *J. Mater. Chem.*, 2005, **15**, 4540–4545.

14 M. Ge, L. Liu, W. Chen and Z. Zhou, *CrystEngComm*, 2012, **14**, 1038–1044.

15 M. K. K. Oo, Y. Yang, Y. Hu, M. Gomez, H. Du and H. Wang, *ACS Nano*, 2012, **6**, 1939–1947.